EPJ Web of Conferences **175**, 06013 (2018) https://doi.org/10.1051/epjconf/201817506013
Lattice 2017

Electromagnetic form factors and axial charge of the nucleon from $N_f = 2 + 1$ Wilson fermions

Dalibor Djukanovic[1], *Tim* Harris[1,2], *Georg M.* von Hippel[2,⋆], *Parikshit M.* Junnarkar[3], *Harvey B.* Meyer[1,2], and *Hartmut* Wittig[1,2]

[1] *Helmholtz Institute Mainz, 55099 Mainz, Germany*
[2] *Institute of Nuclear Physics, University of Mainz, 55099 Mainz, Germany*
[3] *Tata Institute of Fundamental Research, 400005 Mumbai, India*

Abstract. We present an update on our determination of the electromagnetic form factors and axial charge of the nucleon from the $N_f = 2 + 1$ CLS ensembles with increased statistics and an additional finer lattice spacing. We also investigate the impact of $O(a)$-improvement of the currents.

1 Introduction

The charges and form factors of the nucleon encode important information about nucleon structure, such as the spatial distribution of charge and quark spin within the nucleon. From both a theoretical and experimental point of view, the electromagnetic form factors and axial charge of the nucleon are especially important: electromagnetic scattering processes are the most important experimental probe of nucleon structure, and the axial charge is known to high precision from nuclear β decay, making its accurate prediction from first principles a crucial benchmark for lattice QCD. Moreover, the persistent discrepancy between the muonic and electronic determinations of the proton charge radius, and the long-standing difficulties of lattice simulations to reproduce the experimental value of the axial charge make lattice determinations of these quantities with fully controlled errors particularly relevant.

Nucleonic charges and form factors are known to be very difficult observables on the lattice, since they suffer both from an exponentially decaying signal-to-noise ratio and from large excited-state contamination, the combination of which makes it difficult to control statistical and systematic errors at the same time. A variety of methods are therefore necessary to obtain reliable results, both by increasing the statistical accuracy of the data at affordable cost, and by eliminating excited-state contamination as far as possible.

Here we present an update on the Mainz effort [1, 2] to measure the electromagnetic form factors and axial charge of the nucleon on the $N_f = 2 + 1$ CLS ensembles with controlled statistical and systematic errors.

⋆Speaker, e-mail: hippel@uni-mainz.de

2 Observables and Methods

2.1 Observables

The isovector nucleon matrix elements of the vector and axial vector currents $V_\mu(x) = \overline{\psi}(x)\gamma_\mu\psi(x)$ and $A_\mu(x) = \overline{\psi}(x)\gamma_\mu\gamma_5\psi(x)$ can be decomposed in terms of the Pauli and Dirac form factors F_1 and F_2, and the axial and induced pseudoscalar form factors G_A and G_P, respectively:

$$\left\langle N, \mathbf{p}', s' \middle| V_\mu(0) \middle| N, \mathbf{p}, s \right\rangle = \bar{u}(\mathbf{p}', s') \left[\gamma_\mu F_1(Q^2) + \frac{\sigma_{\mu\nu} Q_\nu}{2m_\mathrm{N}} F_2(Q^2) \right] u(\mathbf{p}, s),$$
$$\left\langle N, \mathbf{p}', s' \middle| A_\mu(0) \middle| N, \mathbf{p}, s \right\rangle = \bar{u}(\mathbf{p}', s') \left[\gamma_\mu\gamma_5 G_\mathrm{A}(Q^2) - i\gamma_5 \frac{Q_\mu}{2m_\mathrm{N}} G_\mathrm{P}(Q^2) \right] u(\mathbf{p}, s).$$

Here we study the Sachs electromagnetic form factors G_E and G_M, which can be written in terms of the Pauli and Dirac form factors as

$$G_\mathrm{E}(Q^2) = F_1(Q^2) - \frac{Q^2}{4m_\mathrm{N}^2} F_2(Q^2),$$
$$G_\mathrm{M}(Q^2) = F_1(Q^2) + F_2(Q^2),$$

and the axial charge, which is given by the axial form factor at zero momentum transfer, $g_\mathrm{A} = G_\mathrm{A}(0)$.

2.2 Improvement

We use the O(a)-improved isovector vector and axial vector currents,

$$A^{12}_{\mathrm{R},\mu}(x) = Z_\mathrm{A}(g_0^2) \left(1 + \tilde{b}_\mathrm{A} \mathrm{tr}(aM_\mathrm{q}) + b_\mathrm{A} am^{12}\right) \left(A^{12}_\mu(x) + c_\mathrm{A}(g_0^2)\tilde{\partial}_\mu P^{12}(x)\right)$$
$$V^{\mathrm{c},12}_{\mathrm{R},\mu}(x) = V^{\mathrm{c},12}_\mu(x) + c^\mathrm{c}_\mathrm{V}(g_0^2)\tilde{\partial}_\nu T^{12}_{\mu\nu}(x)$$

in the notation of [3] where $V^{\mathrm{c},12}_\mu(x)$ is the point-split vector current which satisfies a lattice vector Ward identity, and consequently whose charge is correctly normalized. The non-perturbative determination of the factors Z_A and c_A has been performed in [4, 5], while b_A and $\tilde{b}_\mathrm{A}$ have been computed non-perturbatively in [3]. The improvement coefficient c_V has been estimated non-perturbatively by imposing the improvement condition for $N_\mathrm{f} = 3$ Wilson fermions derived from chiral Ward identities [6]

$$\int \mathrm{d}^3y \, \langle \delta S^{12} A^{23}_{\mathrm{R},i}(y^0, \mathbf{y}) V^{31}_i(0) \rangle = \int \mathrm{d}^3y \, \langle V^{\mathrm{c},13}_{\mathrm{R},i}(y^0, \mathbf{y}) V^{31}_i(0) \rangle$$

where

$$\delta S^{12} = -\int_{t_a}^{t_b} \mathrm{d}x^0 \int \mathrm{d}^3x \left(2m^{12} P^{12}_\mathrm{R}(x) - \partial_\mu A^{12}_{\mathrm{R},\mu}(x)\right)$$

and for any $t_a < y^0 < t_b$ and any $m^3 > 0$. The resulting preliminary value are $c^\mathrm{c}_\mathrm{V} = 0.23(3), 0.41(3)$ for $\beta = 3.4, 3.55$ respectively. The tree-level value $c^\mathrm{c}_\mathrm{V} = 0.5$ is used for $\beta = 3.7$.

Table 1. CLS ensembles used in this work

Ensemble	a [fm]	m_π [MeV]	L/a	$m_\pi L$	N_{meas} per t_s	t_s/a
H102	0.086	350	32	4.9	7988	{12, 14, 16}
H105		280	32	3.9	55348	{12, 14, 16}
C101		220	48	4.7	33344	{12, 14, 16}
N200	0.064	280	48	4.4	20412	{12, 14, 16, 18, 20, 22}
D200		200	64	4.2	32672	{16, 18, 20, 22}
J303	0.05	280	64	4.1	5840	{20, 22, 24, 26}

2.3 Gauge Ensembles

We use the lattice ensembles listed in table 1 in this work, which were generated as part of the Coordinated Lattice Simulations (CLS) effort [7] using $N_f = 2 + 1$ dynamical flavours of $O(a)$-improved Wilson fermions, the tree-level Symanzik gauge action, open boundary conditions in time to combat large autocorrelations in the topological charge when approaching the continuum limit [8], and a twisted-mass regulator to prevent problems with (near-)exceptional configurations [9].

Since last year's progress report [2], we have added an additional finer lattice spacing to better control the continuum extrapolation, and significantly increased the statistics on most ensembles, as well as implemented the $O(a)$ improvement of the vector current (cf. section 2.2).

2.4 Measurements

We compute two-point functions

$$C_2(t;\mathbf{p}) = \sum_{\mathbf{x}} \mathrm{e}^{i\mathbf{p}\cdot\mathbf{x}} \Gamma_{\alpha\beta} \left\langle N^\beta(\mathbf{x},t)\overline{N}^\alpha(0)\right\rangle \tag{1}$$

and (using sequential propagators in the fixed-sink setup) three-point functions

$$C_{3,J}((t,t_s;\mathbf{q}) = \sum_{\mathbf{x},\mathbf{y}} \mathrm{e}^{i\mathbf{q}\cdot\mathbf{y}} \Gamma_{\alpha\beta} \left\langle N^\beta(\mathbf{x},t_s) J(\mathbf{y},t) \overline{N}^\alpha(0)\right\rangle, \tag{2}$$

where the nucleon sources and sinks are Wuppertal smeared [10] using APE smeared links [11] to improve the overlap with the ground state. Forming the ratios [12]

$$R_J(t,t_s;\mathbf{q}) = \frac{C_{3,J}(t,t_s;\mathbf{q})}{C_2(t_s;\mathbf{q})} \sqrt{\frac{C_2(t_s-t;\mathbf{q})C_2(t;\mathbf{0})C_2(t_s;\mathbf{0})}{C_2(t_s-t;\mathbf{0})C_2(t;\mathbf{q})C_2(t_s;\mathbf{q})}} \tag{3}$$

which were found to be more advantageous than possible alternatives [13], we can determine effective form factors via

$$\mathrm{Re}\, R_{V_0}(t,t_s;\mathbf{q}) = \sqrt{\frac{m_\mathrm{N}+E_\mathbf{q}}{2E_\mathbf{q}}} G_\mathrm{E}^\mathrm{eff}(t,t_s;Q^2) \tag{4}$$

$$\mathrm{Re}\, R_{V_i}(t,t_s;\mathbf{q}) = \frac{\epsilon_{ij3}q_j}{\sqrt{2E_\mathbf{q}(E_\mathbf{q}+m_\mathrm{N})}} G_\mathrm{M}^\mathrm{eff}(t,t_s;Q^2) \tag{5}$$

$$\mathrm{Im}\, R_{A_3}(t,t_s;\mathbf{0}) = g_\mathrm{A}^\mathrm{eff}(t,t_s) \tag{6}$$

for baryons polarized using $\Gamma = \frac{1}{2}(1+\gamma_0)(1+i\gamma_5\gamma_3)$.

In order to address the signal-to-noise problem of baryonic correlation functions, we employ all-mode-averaging (AMA) with a truncated solver [14] in order to obtain large statistics at moderate expense by computing

$$O^{\mathrm{AMA}} = \frac{1}{N_G}\sum_{g\in G}^{N_G} O^{(\mathrm{appx})\,g} + \frac{1}{N_{\mathrm{org}}}\sum_{f\in G}^{N_{\mathrm{org}}} \underbrace{\left[O^f - O^{(\mathrm{appx})\,f}\right]}_{\text{bias correction}} \tag{7}$$

where the cheap approximate evaluations $O^{(\mathrm{appx})g}$ computed with the truncated solver are averaged over N_G source positions, whereas the precise evaluations O^f used to correct for the bias in the approximation are averaged only over $N_{\mathrm{org}} \ll N_G$ source positions. We note that AMA has been found to be well compatible with the deflated SAP-preconditioned solver used in the openQCD code if the parameters are tuned appropriately [15].

2.5 Excited-State Analysis

At short time separations t, t_s, excited states contribute significantly to the effective form factors through the spectral decomposition of the two- and three-point functions,

$$G_X^{\mathrm{eff}}(t,t_s) = G_X + \sum_{n>1}\left(a_n \mathrm{e}^{-(E_n-E_1)t} + b_n \mathrm{e}^{-(E'_n-E'_1)(t_s-t)} + \ldots\right). \tag{8}$$

For the source-sink separations $t_s \gtrsim 1.0$ fm used in this work, the excited-state contributions are still non-negligible at $t = t_s/2$; in particular, the data show no evidence of reaching a reliable plateau.

To address this problem, and to check whether excited-state effects are under control, we use two different methods, namely

- **Two-state fits**, where we perform an explicit fit assuming that the first excited state dominates the deviations from a plateau, and the
- **Summation method**, which is based on eliminating the t-dependence using the summed ratios [16]

$$S_X(t_s) \equiv \sum_{t=a}^{t_s-a} G_X^{\mathrm{eff}}(t,t_s) = C + t_s G_X + O(\mathrm{e}^{-(E_2-E_1)t_s}), \tag{9}$$

  which allows extracting G_X from a straight-line fit to $S_X(t_s)$ at moderate values of t_s, albeit at the expense of increased statistical errors.

For the axial charge g_{A}, we also use a **many-state fit** ansatz [17] based on the observation that is this case the coefficients $a_n = b_n$ are slowly varying and the energy levels $E'_n = E_n$ are close to those of a free nucleon-pion system in order to enable an explicit fit incorporating contributions from many excited states.

3 Results

We have extracted the Sachs electromagnetic form factors and axial charge using each of the methods discussed above on each of the CLS ensembles listed in Table 1. The results from the two-state and summation methods, and where applicable the many-states method, agreed within errors on most ensembles, indicating that excited-state effects are not dominant (cf. Fig. 1).

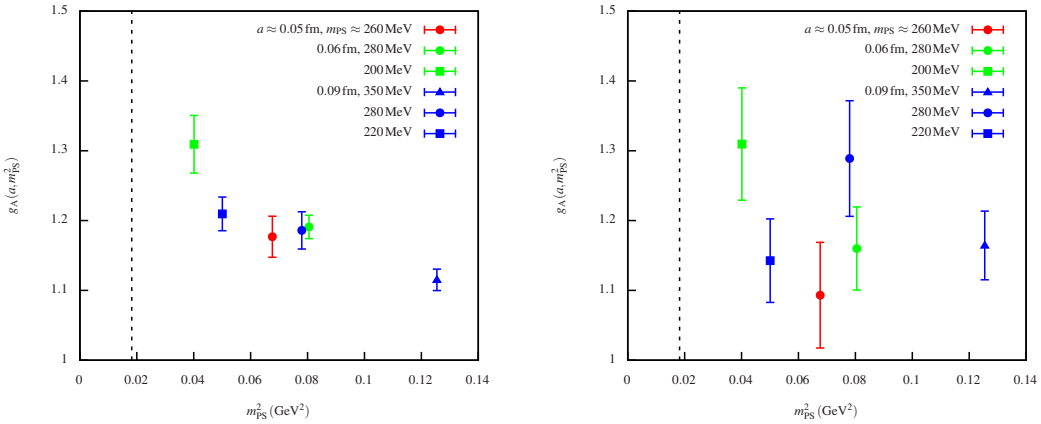

Figure 1. The pion-mass dependence of the axial charge using the two-state (left panel) and summation (right panel) methods, respectively. Within errors, both methods agree.

Comparing the matrix elements for improved and unimproved currents, we find that improvement moves the form factors closer to the experimental curves (cf. Fig. 2), but does not reduce the difference between the final results obtained at different lattice spacings (cf. Fig. 3).

Overall, we find no appreciable trend in the lattice spacing for any of the observables studied here (cf. right column of Fig. 4). Concerning the chiral trend, we do find an approach to the experimental results for the form factors as the pion mass is lowered (cf. left column of Fig. 4). A full chiral and continuum extrapolation is left for a future publication.

4 Outlook

We are working on finalizing our results for the electromagnetic form factors and axial charge of the nucleon from the CLS 2 + 1 flavour ensembles. In particular, we plan to add additional pion mass points at the finest lattice spacing in order to perform a fully controlled chiral and continuum extrapolation. We are also looking into adding the generalized pencil-of-functions (GPOF) method as an additional procedure for removing excited-state contaminations.

On the same set of ensembles, we have also measured the three-point functions required to determine a number of further observables, such as the axial form factors $G_{\mathrm{A}}(Q^2)$ and $G_{\mathrm{P}}(Q^2)$ at $Q^2 > 0$, and the scalar and tensor charges g_{S} and g_{T}, as well as some additional structure observables, including the average quark-momentum fraction $\langle x \rangle$ [18].

Our current plans to extend the scope of this investigation include adding a point at the physical pion mass [19], and in the longer term including isospin-breaking effects [20] and isoscalar form factors.

Acknowledgements: Our calculations were performed on the "Clover" HPC cluster at Helmholtz Institute Mainz, and on the MOGON-II HPC cluster at the University of Mainz. We thank our colleagues in the Coordinated Lattice Simulations (CLS) effort [https://wiki-zeuthen.desy.de/CLS/CLS] for the joint generation of the gauge field ensembles on which the computation described here is based.

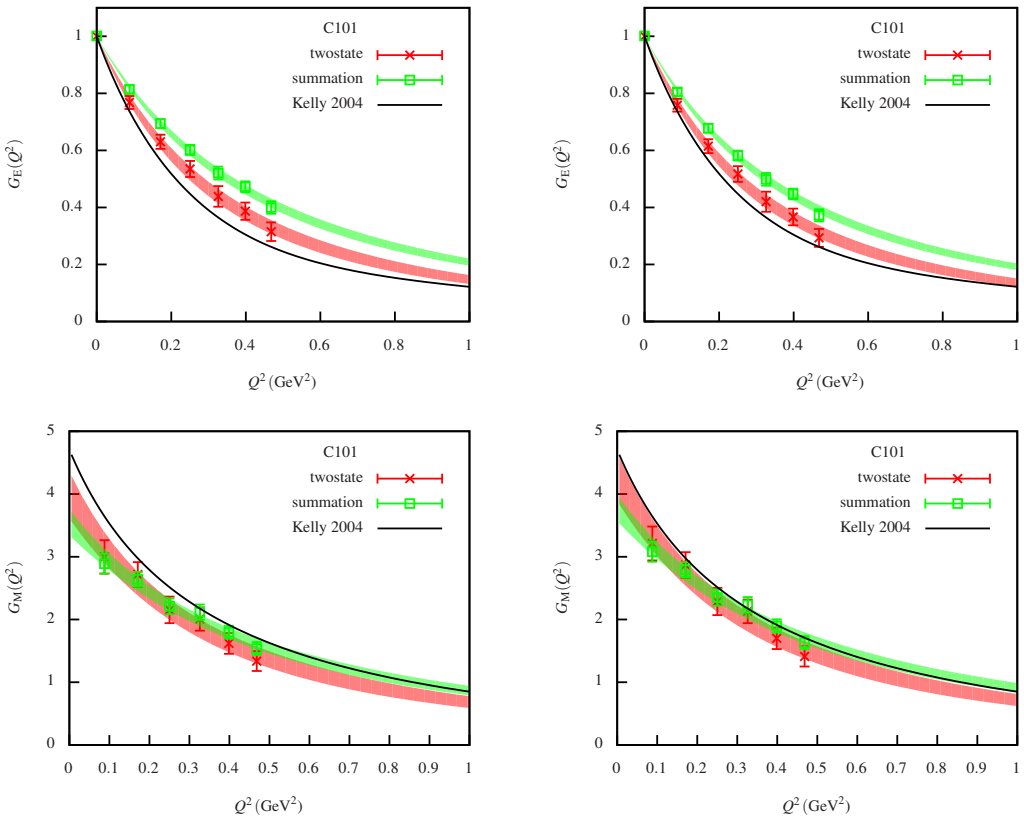

Figure 2. An illustration of the effect of the improvement of the vector current on the Sachs electric (top row) and magnetic (bottom row) form factors (left column: unimproved, right column: improved). Improvement moves the results closer to the Kelly parameterization.

References

[1] D. Djukanovic, T. Harris, G. von Hippel, P. Junnarkar, H.B. Meyer, H. Wittig, PoS **LATTICE2015**, 137 (2016), 1511.07481

[2] D. Djukanovic, T. Harris, G. von Hippel, P. Junnarkar, H.B. Meyer, H. Wittig, PoS **LATTICE2016**, 167 (2017), 1611.07918

[3] P. Korcyl, G.S. Bali, Phys. Rev. **D95**, 014505 (2017), 1607.07090

[4] J. Bulava, M. Della Morte, J. Heitger, C. Wittemeier, Phys. Rev. **D93**, 114513 (2016), 1604.05827

[5] J. Bulava, M. Della Morte, J. Heitger, C. Wittemeier, Nucl. Phys. **B896**, 555 (2015), 1502.04999

[6] T. Bhattacharya, S. Chandrasekharan, R. Gupta, W.J. Lee, S.R. Sharpe, Phys. Lett. **B461**, 79 (1999), hep-lat/9904011

[7] M. Bruno et al. (CLS), JHEP **02**, 043 (2015), 1411.3982

[8] M. Lüscher, S. Schaefer, JHEP **07**, 036 (2011), 1105.4749

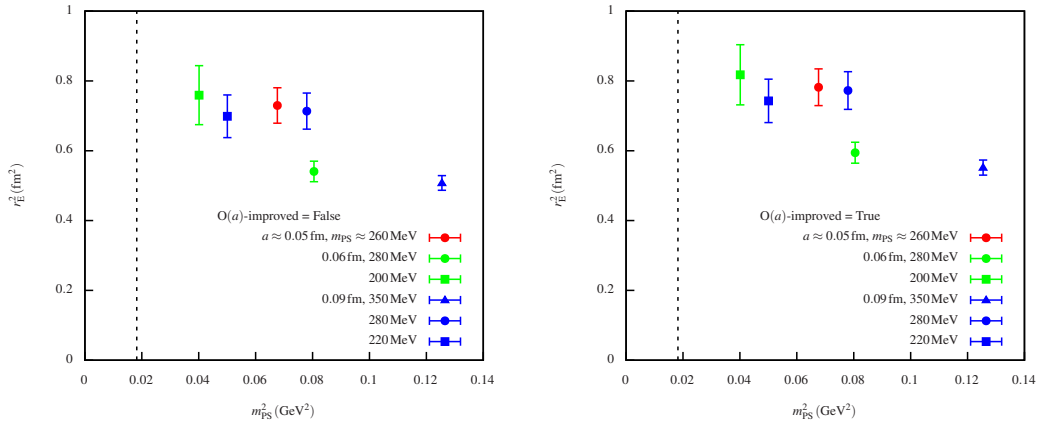

Figure 3. The pion-mass dependence of the electric charge radius of the nucleon using the unimproved (left panel) and improved (right panel) vector current. Improvement leads to larger radii, but does not appear to reduce the already very weak lattice spacing dependence.

[9] M. Lüscher, S. Schaefer, Comput. Phys. Commun. **184**, 519 (2013), 1206.2809
[10] S. Güsken, U. Löw, K.H. Mütter, R. Sommer, A. Patel, K. Schilling, Phys. Lett. **B227**, 266 (1989)
[11] M. Albanese et al. (APE), Phys. Lett. **B192**, 163 (1987)
[12] M. Göckeler et al. (QCDSF), Phys. Rev. **D71**, 034508 (2005), hep-lat/0303019
[13] C. Alexandrou et al. (ETMC), PoS **LATTICE2008**, 139 (2008), 0811.0724
[14] T. Blum, T. Izubuchi, E. Shintani, Phys. Rev. **D88**, 094503 (2013), 1208.4349
[15] G. von Hippel, T.D. Rae, E. Shintani, H. Wittig, Nucl. Phys. **B914**, 138 (2017), 1605.00564
[16] L. Maiani, G. Martinelli, M.L. Paciello, B. Taglienti, Nucl. Phys. **B293**, 420 (1987)
[17] M.T. Hansen, H.B. Meyer, *On the effect of excited states in lattice calculations of the nucleon axial charge* (2016), 1610.03843
[18] K. Ottnad et al., *Nucleon average quark momentum fraction with $N_f = 2 + 1$ Wilson fermions*, in *Proceedings, 35th International Symposium on Lattice Field Theory (Lattice2017): Granada, Spain* (2018)
[19] D. Mohler et al., *CLS 2 + 1 flavor simulations at physical light- and strange-quark masses*, in *Proceedings, 35th International Symposium on Lattice Field Theory (Lattice2017): Granada, Spain* (2018)
[20] A. Risch et al., *Towards leading isospin breaking effects in mesonic masses with O(a) improved Wilson fermions*, in *Proceedings, 35th International Symposium on Lattice Field Theory (Lattice2017): Granada, Spain* (2018)

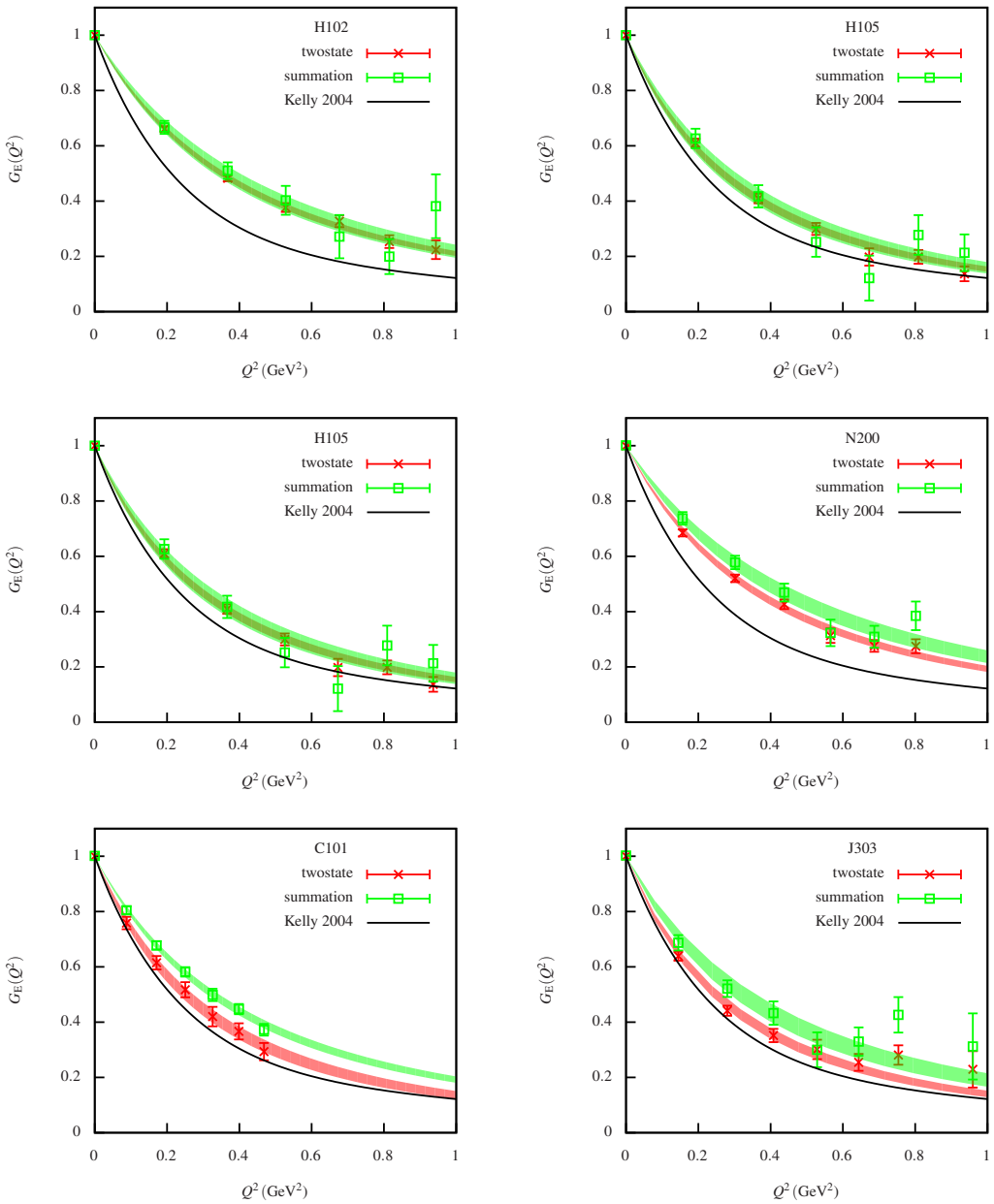

Figure 4. The Sachs electric form factor $G_E(Q^2)$; the left column shows the chiral trend at a lattice spacing of $a = 0.086$ fm, and the right column shows the lattice-spacing dependence at a pion mass of $m_\pi = 280$ MeV.